JPE 16-4-18

http://dx.doi.org/10.6113/JPE.2016.16.4.1415
ISSN(Print): 1598-2092 / ISSN(Online): 2093-4718

A Real-Time Method for the Diagnosis of Multiple Switch Faults in NPC Inverters Based on Output Currents Analysis

Mohsen Bandar Abadi[†], André M. S. Mendes[*], and Sérgio M. A. Cruz[*]

[†,*]Instituto de Telecomunicações and Department of Electrical and Computer Engineering, University of Coimbra, Coimbra, Portugal

Abstract

This paper presents a new approach for fault diagnosis in three-level neutral point clamped inverters. The proposed method is based on the average values of the positive and negative parts of normalized output currents. This method is capable of detecting and locating multiple open-circuit faults in the controlled power switches of converters in half of a fundamental period of those currents. The implementation of this diagnostic approach only requires two output currents of the inverter. Therefore, no additional sensors are needed other than the ones already used by the control system of a drive based on this type of converter. Moreover, through the normalization of currents, the diagnosis is independent of the load level of the converter. The performance and effectiveness of the proposed diagnostic technique are validated by experimental results obtained under steady-state and transient conditions.

Key words: AC drive, Fault location, Multiple faults, NPC inverter, Open-circuit faults

NOMENCLATURE

$x \in \{A,B,C\}$	Inverter leg index
i_x	Inverter output current of leg x
$i_{x.n}$	i_x normalized
$i_{x.n}^+$, $i_{x.n}^-$	Positive and negative parts of $i_{x.n}$
$i_{x.n.av}^+$, $i_{x.n.av}^-$	Average values of $i_{x.n}^+$ and $i_{x.n}^-$
I_{av}^{th1+} , I_{av}^{th2+}	First and second threshold values for $i_{x.n.av}^+$
I_{av}^{th1-} , I_{av}^{th2-}	First and second threshold values for $i_{x.n.av}^-$
I^{th+} , I^{th-}	Threshold values for $i_{x.n}$
e_x^+ , e_x^- , f_x	Diagnostic variables
F_T^{1st} , F_T^{2nd}	Time of the occurrence of the first and second faults
F_{pair}^{1st} , F_{pair}^{2nd}	First and second faulty pair number
F_{switch}^{1st} , F_{switch}^{2nd}	First and second faulty switch number

Manuscript received Nov. 27, 2015; accepted Mar. 27, 2016
Recommended for publication by Associate Editor Kyo-Beum Lee.
[†]Corresponding Author: m.b.abadi@ieee.org
Tel: +351-918582872, University of Coimbra, Coimbra, Portugal
[*]Instituto de Telecomunicações and Department of Electrical and Computer Engineering, University of Coimbra, Portugal

I. INTRODUCTION

Multilevel converters are considered a very attractive solution for both rectifier and inverter stages of power converters used in medium-voltage and high-power drives [1], [2]. Higher voltage blocking capability, reduced output harmonic content, lower switching losses, higher power quality waveforms and lower voltage stresses are some of the advantages of multilevel converters when compared to conventional two-level converters [3], [4].

Three-level neutral point clamped (3LNPC) inverters belong in a category of multilevel converters that are increasingly being used in industry [5], [6]. Wind energy conversion [7], photovoltaic conversion [8] and multiphase AC drives [9] are some of the applications of 3LNPC inverters.

However, due to the complexity of the 3LNPC topology, and the requirement of a large number of switches and gate drivers, the probability of the occurrence of a fault is not negligible [10].

One common type of fault in the power switches of a converter is an IGBT open-circuit (OC) fault [11], [12]. This kind of fault can arise if the IGBT rated parameters, such as the

rated collector-emitter voltage V_{ce} or the rated collector current I_c, are exceeded, or when the gate driver unit fails [13].

In standard applications, after the occurrence of a fault in one or more of the power switches, the converter is stopped. However, in recent years, there has been an increase in the demand for nonstop service in many industrial applications. To achieve this goal, the power converter should be able to operate continuously, even during fault conditions, being that one of the main aims of fault tolerance [14].

To implement fault tolerant control strategies in a converter, the use of a reliable real-time diagnostic system is required. Furthermore, a diagnostic system with the ability to identify the faulty element has some advantages such as the ability to select the best fault tolerant control strategy, or the reduction of the inverter repair time as well as the associated repair cost.

This work gives special attention to the OC faults in IGBTs since in many cases this type of fault is not detected by the IGBT gate driver circuit or by converter protection systems. If an OC fault is not detected and the protection system of the converter does not actuate, it will continue to run and can be the source of other faults [15].

Several approaches were proposed for fault diagnosis in 3LNPC inverters. A method for detecting the OC faults in 3LNPC inverters by measuring the pole voltage is presented in [16].A method for OC fault diagnosis in grid-connected 3LNPC inverters based on the output line currents is proposed in [10]. In [17], a method for detection of the OC faults in the 3LNPC back-to-back converters used in permanent magnet synchronous generators (PMSG) is proposed.

A new diagnostic method based on the average current Park's Vector (ACPV) is proposed in [18], [19]. This method does not need any extra sensors and is able to identify the single faulty IGBT in a 3LNPC inverter.

The state of the art in fault diagnosis in 3LNPC inverters indicates that all of the proposed approaches for fault diagnosis in 3LNPC converters only pay attention to the occurrence of a single fault and do not have the ability to identify simultaneous failures. Due to the high number of power switches, the probability of the occurrence of the multiple faults in 3LNPC inverters is not negligible. If more than one OC fault is present, in some cases the implementation of fault tolerant control strategies is impossible. In such cases, the diagnostic method should be able to diagnose multiple IGBT OC faults to avoid running the reconfiguration by the fault tolerant system. Otherwise, the results obtained by the fault diagnostic system lead to run the fault tolerant strategy in an inappropriate way. This can be the cause of further damage in the other healthy devices of the inverter.

In order to overcome this limitation, this paper presents a new fault diagnostic method based on the average values of the positive and negative parts of the normalized motor line current waveforms. The proposed diagnostic approach is able to identify multiple OC faults in the controlled power switches of 3LNPC inverters.

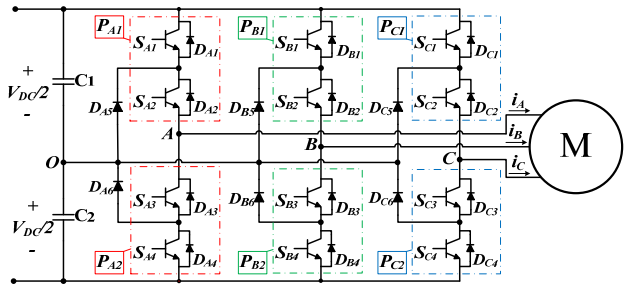

Fig. 1. Schematic representation of a 3LNPC inverter.

The remaining part of this paper is structured as follows. Section II presents the 3LNPC operation under normal and IGBT OC fault conditions. Section III presents the proposed technique for the diagnosis of OC faults. Details of the experimental setup and discussion of the experimental results are presented in Section IV, which includes three subsections with results for single faults, multiple faults and load variations. Finally, Section V presents the main conclusions of this work.

II. 3LNPC Drive Under Healthy and Faulty Conditions

The topology of a 3LNPC inverter is shown in Fig. 1 [20]. It consists of three legs, with four active switches per leg, labeled S_{x1}, S_{x2}, S_{x3}, S_{x4}, four freewheeling diodes labeled D_{x1}, D_{x2}, D_{x3}, D_{x4} and two clamping diodes labeled D_{x5} and D_{x6} (x means leg A, B or C). Each leg includes 2 IGBT pairs, P_{x1} and P_{x2}, as shown in Fig. 1. Moreover, in this work, S_{x1} and S_{x4} are the outer switches while S_{x2} and S_{x3} are the inner switches. The active switches are IGBTs and the DC-bus has 2 capacitors, which provide the middle point "O".

The IGBTs of each inverter leg provide three different switching states, designated as 1, 0, and -1, according to the information listed in TABLE I. More information about the operating modes of inverter legs can be found in [21].

Fig. 2 shows the 6 available current paths for each leg according to the current direction and the corresponding state [16]. The unavailable switching state(s) and current path(s) in leg x after the occurrence of an OC fault are listed in TABLE II for 10 different faulty switch combinations (conditions 1 to 4 for a single fault, and conditions 5 to 10 for double faults).

When an inverter leg is in switching state 1 and the output current is positive (according to Fig. 2), if a fault occurs in S_{x1}, the output terminal of the affected leg is disconnected from the positive terminal of the DC bus and is connected to terminal O. Hence, current path 1 is changed to current path 2. As a result, i_x has a smaller amplitude when compared with the normal operation of that leg. When a fault occurs in S_{x2}, no positive current i_x flows to the load (motor). Thus, the behavior of the

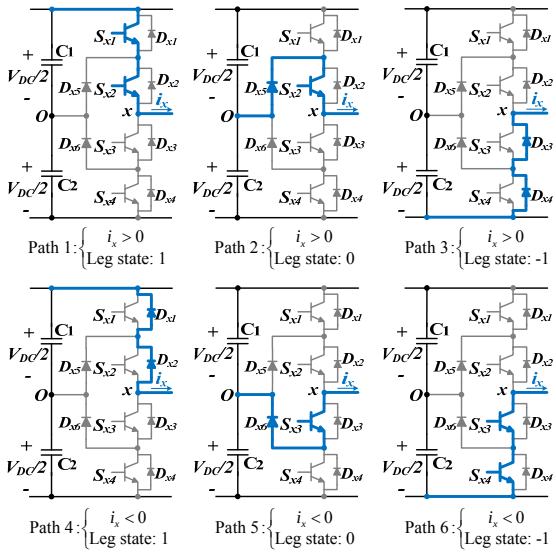

Fig. 2. Current paths according to the current direction and leg state.

TABLE I
SWITCHING STATES OF LEG X

State of leg x	IGBTs states				Pole voltage	Current path	
	S_{x1}	S_{x2}	S_{x3}	S_{x4}	(v_{xO})	i_x>0	i_x<0
1	on	on	off	off	+V_{DC} /2	1	4
0	off	on	on	off	0	2	5
-1	off	off	on	on	-V_{DC} /2	3	6

TABLE II
INVERTER LEG SITUATION AFTER AN OC FAULT IN LEG X

Condition number	IGBT situation of leg x				Unavailable leg state(s)	Unavailable current path(s)
	S_{x1}	S_{x2}	S_{x3}	S_{x4}		
1	OC	ok	ok	ok	1	1
2	ok	OC	ok	ok	1, 0	1, 2
3	ok	ok	OC	ok	0, -1	5, 6
4	ok	ok	ok	OC	-1	6
5	OC	OC	ok	ok	1, 0	1, 2
6	OC	ok	OC	ok	1, 0, -1	1, 5, 6
7	OC	ok	ok	OC	1, -1	1, 6
8	ok	OC	OC	ok	1, 0, -1	1, 2, 5, 6
9	ok	OC	ok	OC	1, 0, -1	1, 2, 6
10	ok	ok	OC	OC	0, -1	5, 6

positive values of i_x depends on whether the fault occurs in an outer IGBT during switching state 1 (small positive current values available) or in an inner IGBT with states 1 or 0 (no positive current values are available).

III. PROPOSED DIAGNOSTIC TECHNIQUE

A new method for the diagnoses of multiple OC faults in a 3LNPC inverter, based on the average values of the positive and negative parts of the line currents, is proposed in this paper.

To obtain a diagnostic method independent of the load condition, the motor line currents $i_A[k]$, $i_B[k]$ and $i_C[k]$ are normalized and $i_{x.n}[k]$ is obtained according to (2), using the magnitude of the motor line current Park's Vector $|\boldsymbol{i}_s[k]|$ obtained by (1). Then, the normalized line current $i_{x.n}[k]$ is split into two parts, one with positive values $i^{+}_{x.n}[k]$ and the other with negative values $i^{-}_{x.n}[k]$, which are determined by (3) and (4), respectively. Thus, the average values of $i^{+}_{x.n}[k]$ and $i^{-}_{x.n}[k]$ are calculated by (5) and (6), respectively, where N is the number of samples in one period of currents, k is the index of a sample, and x is the inverter leg index.

$$\begin{cases} i_{s.d}[k] = \frac{2}{3} i_A[k] - \frac{1}{3}(i_B[k] + i_C[k]) \\ i_{s.q}[k] = \frac{1}{\sqrt{3}}(i_B[k] - i_C[k]) \\ \boldsymbol{i}_s[k] = i_{s.d}[k] + j.i_{s.q}[k] = |i_s[k]| \angle \theta_s \end{cases} \quad (1)$$

$$i_{x.n}[k] = \frac{i_x[k]}{|\boldsymbol{i}_s[k]|} \quad , \quad x \in \{A, B, C\} \quad (2)$$

$$i^{+}_{x.n}[k] = \begin{cases} i_{x.n}[k] \Leftarrow & i_{x.n}[k] > 0 \\ 0 \Leftarrow & i_{x.n}[k] \le 0 \end{cases} \quad (3)$$

$$i^{-}_{x.n}[k] = \begin{cases} 0 \Leftarrow & i_{x.n}[k] \ge 0 \\ i_{x.n}[k] \Leftarrow & i_{x.n}[k] < 0 \end{cases} \quad (4)$$

$$i^{+}_{x.n.av}[k] = \frac{1}{N} \sum_{j=k-N}^{k} i^{+}_{x.n}[j] \quad (5)$$

$$i^{-}_{x.n.av}[k] = \frac{1}{N} \sum_{j=k-N}^{k} i^{-}_{x.n}[j] \quad (6)$$

Under healthy conditions, $i^{+}_{x.n}[k]$ and $i^{-}_{x.n}[k]$ signals are equivalent to a half-wave rectified signal. Therefore, $i^{+}_{x.n.av}[k] \approx 0.318$ pu and $i^{-}_{x.n.av}[k] \approx -0.318$ pu.

After the occurrence of an OC fault in one of the IGBTs located in P_{x1} (S_{x1} or S_{x2}), $i^{+}_{x.n.av}[k]$ decreases and $i^{-}_{x.n.av}[k]$ changes a little but is still far away from the threshold. In the presence of an OC fault in one of the IGBTs located in P_{x2} (S_{x3} or S_{x4}), $i^{-}_{x.n.av}[k]$ increases and $i^{+}_{x.n.av}[k]$ changes a little but is still far away from the threshold. The evolution of $i^{+}_{x.n.av}[k]$ and $i^{-}_{x.n.av}[k]$ under an OC fault can be used for fault detection and the identification of the faulty IGBT pair (F_{pair}).

In order to implement the diagnostic algorithm in a 3LNPC digital controller and to have the ability to detect and locate the faulty IGBT, it is necessary to use the diagnostic variables $e^{+}_{x}[k]$, $e^{-}_{x}[k]$ and $f_x[k]$ ($x \in \{A, B, C\}$).

According to (7) and (8), the variables $e^{+}_{x}[k]$ and $e^{-}_{x}[k]$ are obtained from the comparison of $i^{+}_{x.n.av}[k]$ and $i^{-}_{x.n.av}[k]$ with the corresponding threshold values I^{th1+}_{av}, I^{th2+}_{av}, I^{th1-}_{av} and I^{th2-}_{av}. According to (9), the variable $f_x[k]$ is obtained from the comparison of $i_{x.n}[k]$ with the threshold values I^{th+} and I^{th-}.

According to (7) and (8), if the inverter operates with no faults, the diagnostic variables $e^{+}_{x}[k]$ and $e^{-}_{x}[k]$ present

TABLE III
DETAILS OF THE USED THRESHOLDS VALUES

Diagnostic variable	Threshold label	Threshold detail	Threshold value
$e_x^+[k]$	I_{av}^{th1+}	First threshold value for $i_{x.n.av}^+$	0.1
	I_{av}^{th2+}	Second threshold value for $i_{x.n.av}^+$	0.01
$e_x^-[k]$	I_{av}^{th1-}	First threshold value for $i_{x.n.av}^-$	-0.1
	I_{av}^{th2-}	Second threshold value for $i_{x.n.av}^-$	-0.01
$f_x[k]$	I^{th+}	Positive threshold value for $i_{x.n}$	0.1
	I^{th-}	Negative threshold value for $i_{x.n}$	-0.1

null values. In addition, under normal conditions, the variable $f_x[k]$ changes between -1, 0 and 1, as shown in (9).

$$e_x^+[k]=\begin{cases}0, & i_{x.n.av}^+[k]>I_{av}^{th1+}\\ 1, & I_{av}^{th2+}<i_{x.n.av}^+[k]\le I_{av}^{th1+}\\ 2, & i_{x.n.av}^+[k]\le I_{av}^{th2+}\end{cases} \quad (7)$$

$$e_x^-[k]=\begin{cases}0, & i_{x.n.av}^-[k]<I_{av}^{th1-}\\ 1, & I_{av}^{th2-}>i_{x.n.av}^-[k]\ge I_{av}^{th1-}\\ 2, & i_{x.n.av}^-[k]\ge I_{av}^{th2-}\end{cases} \quad (8)$$

$$f_x[k]=\begin{cases}1, & i_{x.n}[k]\ge I^{th+}\\ 0, & I^{th+}<i_{x.n}[k]<I^{th-}\\ -1, & i_{x.n}[k]\le I^{th-}\end{cases} \quad (9)$$

Details of the threshold values used in this paper are listed in TABLE III. These threshold values have been chosen by a trial and error procedure for several faulty conditions of the 3LNPC. Later they were validated by simulation and experimental diagnostic results. Since $i_{x.n}[k]$, $i_{x.n.av}^+[k]$ and $i_{x.n.av}^-[k]$ are normalized values, the employed threshold values are independent of the operating conditions of the inverter and do not need to be adjusted for each specific operating condition.

For fault detection and identification F_{pair}, $i_{x.n.av}^+[k]$ and $i_{x.n.av}^-[k]$ are compared with two threshold values $I_{av}^{th1+}=0.1$ and $I_{av}^{th1-}=-0.1$, respectively. These threshold values represent 31% of the values of $i_{x.n.av}^+[k]$ and $i_{x.n.av}^-[k]$ under healthy conditions. Therefore, there is a sufficient safety margin to avoid false alarms due to more severe or unusual working conditions such as during transient operation or unbalanced load conditions.

For discrimination between the outer and inner IGBT faults in an IGBT pair, $i_{x.n}[k]$ is compared with two threshold values $I^{th+}=0.1$ and $I^{th-}=-0.1$ (10% of the maximum value of $i_{x.n}$ under healthy conditions), while $i_{x.n.av}^+[k]$ and $i_{x.n.av}^-[k]$ are compared with two threshold values $I_{av}^{th2+}=0.01$ and $I_{av}^{th2-}=-0.01$ (3.1% of the values $i_{x.n.av}^+[k]$ and $i_{x.n.av}^-[k]$, under healthy conditions).

To address the detection and identification of F_{pair}, the

TABLE IV
LOOKUP TABLE FOR FAULTY PAIR IDENTIFICATION

e_A^+	e_A^-	e_B^+	e_B^-	e_C^+	e_C^-	F_{Pair} Number	F_{Pair} Label	F_{leg} Number	F_{leg} Label
≥1	--	--	--	--	--	1	P_{A1}	1	A
--	≥1	--	--	--	--	2	P_{A2}		
--	--	≥1	--	--	--	3	P_{B1}	2	B
--	--	--	≥1	--	--	4	P_{B2}		
--	--	--	--	≥1	--	5	P_{C1}	3	C
--	--	--	--	--	≥1	6	P_{C2}		

TABLE V
LOOKUP TABLE FOR IDENTIFICATION OF THE FAULTY IGBT(S)

F_{pair}	f_A	e_A^+	e_A^-	f_B	e_B^+	e_B^-	f_C	e_C^+	e_C^-	F_{switch} Number	F_{switch} Label
P_{A1}	1	--	--	--	--	--	--	--	--	1	S_{A1}
	--	2	--	--	--	--	--	--	--	2	S_{A2}
P_{A2}	--	--	2	--	--	--	--	--	--	3	S_{A3}
	-1	--	--	--	--	--	--	--	--	4	S_{A4}
P_{B1}	--	--	--	1	--	--	--	--	--	5	S_{B1}
	--	--	--	--	2	--	--	--	--	6	S_{B2}
P_{B2}	--	--	--	--	--	2	--	--	--	7	S_{B3}
	--	--	--	-1	--	--	--	--	--	8	S_{B4}
P_{C1}	--	--	--	--	--	--	1	--	--	9	S_{C1}
	--	--	--	--	--	--	--	2	--	10	S_{C2}
P_{C2}	--	--	--	--	--	--	--	--	2	11	S_{C3}
	--	--	--	--	--	--	-1	--	--	12	S_{C4}

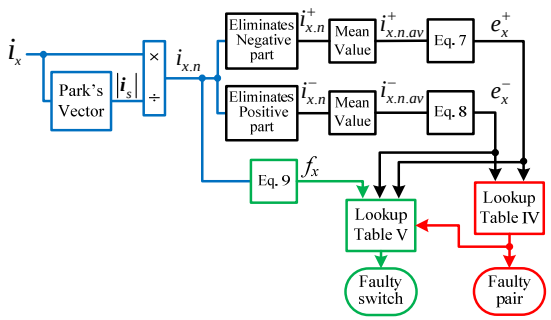

Fig. 3. Block diagram of the proposed diagnostic algorithm.

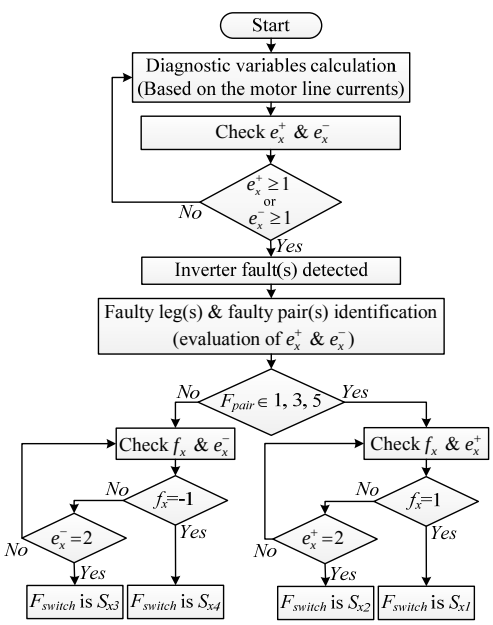

Fig. 4. Flowchart of the proposed diagnostic algorithm.

values of $e_x^+[k]$ and $e_x^-[k]$ are used, as presented in TABLE IV. If $e_x^+[k]$ or $e_x^-[k]$ present a value that is higher than 0, a fault is detected and both F_{pair} and the faulty leg (F_{leg}) are immediately identified. The symbol "--" in TABLE IV means that the variable value is irrelevant for the diagnostic process.

After F_{pair} identification, F_{pair} together with the values of $f_x[k]$, $e_x^+[k]$ and $e_x^-[k]$ are necessary to identify F_{switch}, as shown in TABLE V. For example, if a fault occurs in the IGBT pair P_{A1}, based on TABLE V, the values of $f_A[k]$ and $e_A^+[k]$ are necessary to identify F_{switch}. If $f_A[k]$ takes the value 1, then $F_{switch}=S_{A1}$, and if $e_A^+[k]$ takes the value 2, $F_{switch}=S_{A2}$.

The block diagram and the flowchart of the proposed OC fault diagnostic procedure are presented in Fig. 3 and Fig. 4, respectively.

IV. Validation of the Diagnostic Approach

A. System under test

To test and validate the proposed diagnostic approach, a 3LNPC motor drive system, comprising an induction motor fed by a 3LNPC converter and controlled by a rotor field oriented control (RFOC) strategy was used.

A simulation model of this system was built in the Matlab/Simulink environment. In this model, the space vector modulation (SVM) technique with even-order harmonic elimination was used [20], [22].

In addition to the simulation model, an experimental setup (Fig. 5) was also built. A 3LNPC inverter prototype was developed, where the power switches are Semix IGBT modules, with SKYPER 32 PRO drivers that constitute an interface between the IGBT modules and the controller. OC faults can be introduced in all of the power switches of the inverter in a controlled way. In the experiments, OC faults were introduced by sending the zero control state to specific IGBTs.

This 3LNPC inverter feeds a WEG W22, 4 kW, 400 V, 50 Hz, 8.12 A, 1435 rpm, three-phase induction motor. The motor and inverter control systems, as well as the diagnostic system, are implemented in a digital controller based on a dSPACE ds1103 platform.

The 3LNPC inverter is supplied by a constant DC voltage of 200 V. The mechanical load of the induction motor is a WEG 4 kW permanent magnet synchronous generator feeding a variable load resistor.

B. Experimental results

In order to assess the proposed diagnostic technique, several IGBT OC faults were introduced into the 3LNPC inverter. Each IGBT OC fault test was conducted for different values of motor load torque and several reference speeds,

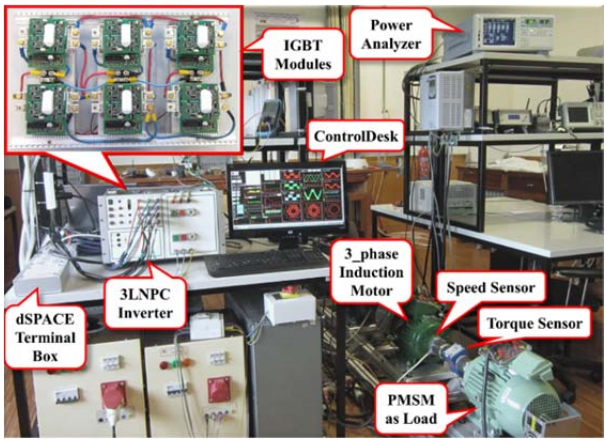

Fig. 5. The experimental setup.

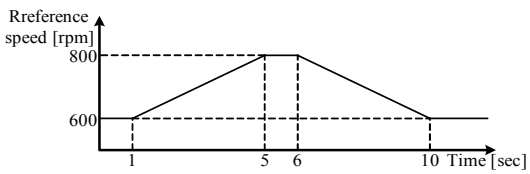

Fig. 6. The employed profile of the reference speed.

under both steady state and transient conditions.

In this subsection, results for different inverter faulty conditions, with single and double IGBT OC faults are presented.

1) Results for a single IGBT OC fault

In this subsection, results for three different single IGBT OC faults are analyzed. The employed reference speed profile for the first and second tests is shown in Fig. 6. In both tests, at t=3 s (in the middle of the acceleration ramp), an OC fault is introduced in the inverter. In the first test, an OC fault is introduced in IGBT S_{A1}. In the second test, the fault is introduced in IGBT S_{A2}.

The motor mechanical speed and load torque evolutions for these faulty conditions are shown in Fig. 7. In these figures, the instant when the fault was introduced is marked with a vertical line labeled F_T. As can be noticed, before the fault occurrence, the motor speed follows the reference and the motor electromagnetic torque is stable with 5 Nm. After t=3 s, both of the results show that the motor is unable to follow the speed reference and the motor torque has oscillations. The figures also show that the oscillations of the motor speed and torque due to S_{A2} fault are higher than those with S_{A1} fault. The motor line current waveforms with an OC fault in the IGBTs S_{A1} and S_{A2} are represented in Fig. 8(a) and Fig. 8(b), respectively.

The diagnosis of these faults is developed in two steps. The first step involves the OC fault detection and the faulty IGBT pair (F_{pair}) identification. For this purpose, TABLE IV is used. After the identification of F_{pair}, it is necessary to check the diagnostic variable values presented in TABLE V, in order to identify the faulty IGBT.

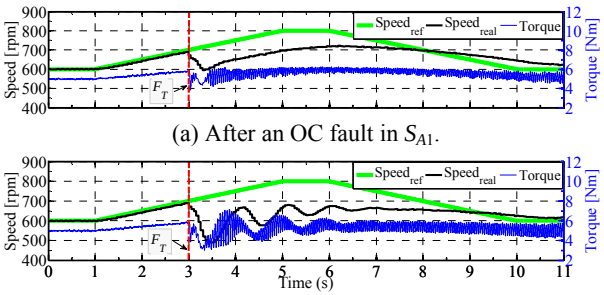

(a) After an OC fault in S_{A1}.

(b) After an OC fault in S_{A2}.

Fig. 7. Transient of motor speed and load torque.

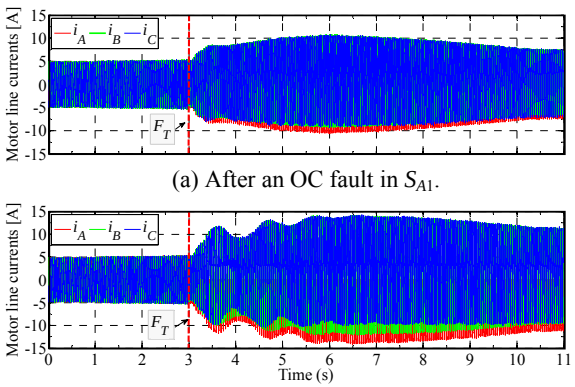

(a) After an OC fault in S_{A1}.

(b) After an OC fault in S_{A2}.

Fig. 8. Transient of motor line currents.

For the case of an OC in S_{A1}, the results are presented in Fig. 9. The zoomed motor line current waveforms around t=3 s are presented in Fig. 9(a). Considering an OC fault at t=3 s in the inverter leg A, Fig. 9(b) shows the normalized current of leg A ($i_{A.n}[k]$) together with the average values of both the positive part ($i^{+}_{\bar{A}.n.av}[k]$) and the negative part ($i^{-}_{\bar{A}.n.av}[k]$). As can be noticed, before the fault occurrence, $i_{A.n}[k]$ has a sinusoidal shape with amplitude of 1 pu and therefore $i^{+}_{\bar{A}.n.av}[k] \approx 0.318$ pu and $i^{-}_{\bar{A}.n.av}[k] \approx -0.318$ pu. After the appearance of the fault, almost all of the positive values of $i_{A.n}[k]$ are eliminated and the value of $i^{+}_{\bar{A}.n.av}[k]$ decreases. When $i^{+}_{\bar{A}.n.av}[k]$ is below the threshold value I^{th1+}_{av} (Fig. 9(b)), $e^{+}_{A}[k]$ takes the value 1 (at t=3.0115 s) as shown in Fig. 9(c). Considering these results, TABLE IV allows the identification of F_{leg}=1 (leg A) and F_{pair}=1 (P_{A1}).

Since F_{pair}=1, there are two possible faulty switches, S_{A1} and S_{A2}. Thus, based on TABLE V, the value of $e^{+}_{A}[k]$ and $f_A[k]$ are necessary to identify the faulty switch. The first time that $f_A[k]$ takes the value of 1 after the faulty pair 1 identification, TABLE V allows for identifying S_{A1} as the faulty IGBT. As can be seen in the diagnostic timeline represented in Fig. 9(d), the IGBT pair number 1 (P_{A1}) and the faulty switch number 1 (S_{A1}) are identified by the algorithm.

For the second test with an OC in S_{A2}, a zoom of Fig. 8(b) around t=3 s, is presented in Fig. 10(a). The results for

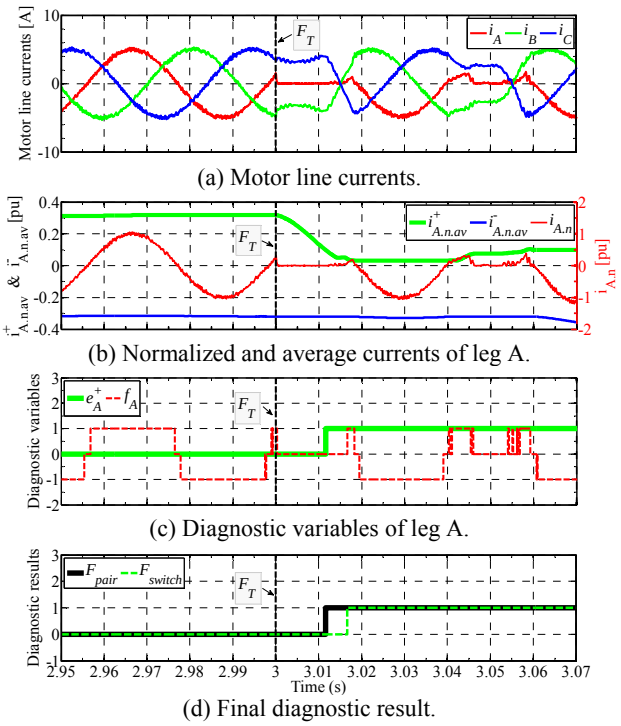

(a) Motor line currents.

(b) Normalized and average currents of leg A.

(c) Diagnostic variables of leg A.

(d) Final diagnostic result.

Fig. 9. Results for the inverter operation with OC fault in S_{A1}.

$i_{A.n}[k]$, $i^{+}_{\bar{A}.n.av}[k]$ and $i^{-}_{\bar{A}.n.av}[k]$ are shown in Fig. 10(b).

After the fault occurrence at t=3 s, the positive part of $i_{A.n}[k]$ is completely eliminated. Therefore, $i^{+}_{\bar{A}.n.av}[k]$ decreases to zero. As observed in Fig. 10(b), $i^{+}_{\bar{A}.n.av}[k]$ decreases to a value below I^{th1+}_{av} at t=3.0115 s. At this point $e^{+}_{A}[k]=1$ (Fig. 10(c)) and the fault is detected. Using these diagnostic variable values as entries in TABLE IV, the identification of the faulty IGBT pair as number 1 (P_{A1}) is achieved (Fig. 10(d)).

After fault detection, taking into account that F_{pair}=P_{A1}, identifying the faulty IGBT is necessary to check the values of $e^{+}_{A}[k]$ and $f_A[k]$. Fig. 10(c) shows that after fault occurrence, $f_A[k]$ changes between -1 and 0, and $e^{+}_{A}[k]$ assumes the value 2 at t=3.0175 s. Considering these values, TABLE V allows for the identification of S_{A2} as the faulty IGBT.

The timeline of the diagnostic process is shown in Fig. 10(d).

In the third test, the capability of the proposed method under unbalanced load conditions (that can be the result of a motor fault for example) is evaluated. To emulate a fault in the motor, an extra resistor is connected in series with phase A. As a consequence of this procedure, the motor line currents became very unbalanced (equivalent to a motor fault with a high severity). Then, under this unbalanced operating condition, an OC fault is introduced in IGBT S_{A1}.

The motor speeds and load torque evolution are shown in Fig. 11(a), where the time of occurrence of the unbalanced load and the IGBT OC fault are marked with two vertical lines

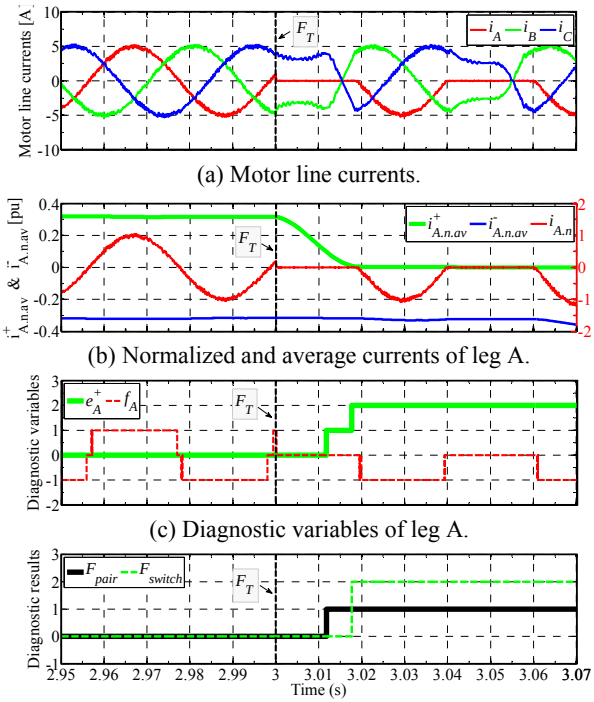

(a) Motor line currents.

(b) Normalized and average currents of leg A.

(c) Diagnostic variables of leg A.

(d) Final diagnostic result.

Fig. 10. Results for the inverter operation with OC fault in S_{A2}.

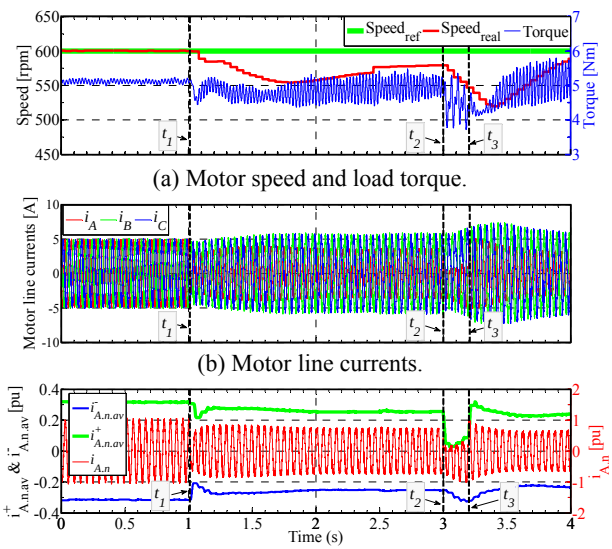

(a) Motor speed and load torque.

(b) Motor line currents.

(c) Normalized and average currents of leg A.

Fig. 11. Results for an OC in S_{A1} under unbalanced operation.

labeled t_1 and t_2, respectively. The vertical line labeled t_3 indicates the instant in time when the OC fault in S_{A1} is eliminated. As shown in this figure, after the occurrence of the motor fault (1 s<t<3 s), the motor speed is unable to follow the corresponding reference value, while the load torque presents oscillations. In the presence of the IGBT OC fault (3 s<t<3.2 s), the amplitude of the torque oscillation increases. The corresponding motor line current waveforms are shown in Fig. 11(b). Fig. 11(c) shows $i_{A.n}[k]$, $i^+_{A.n.av}[k]$ and $i^-_{A.n.av}[k]$.

After the occurrence of the motor fault (1 s<t<3 s), the amplitude of $i_{A.n}[k]$ decreases. Consequently, the values of $i^+_{A.n.av}[k]$ and $i^-_{A.n.av}[k]$ change. However, they never reach the corresponding threshold values (I^{th1+}_{av} and I^{th1-}_{av}). Therefore, the diagnostic process does not provide any false alarms under this unbalanced operating condition. As can be observed in Fig. 11(c), in the presence of an IGBT OC fault (3 s<t<3.2 s), the value of $i^+_{A.n.av}[k]$ is below I^{th1+}_{av}. After the elimination of the IGBT fault (t>3.2 s), the value of $i^+_{A.n.av}[k]$ increase to a value higher than I^{th1+}_{av}.

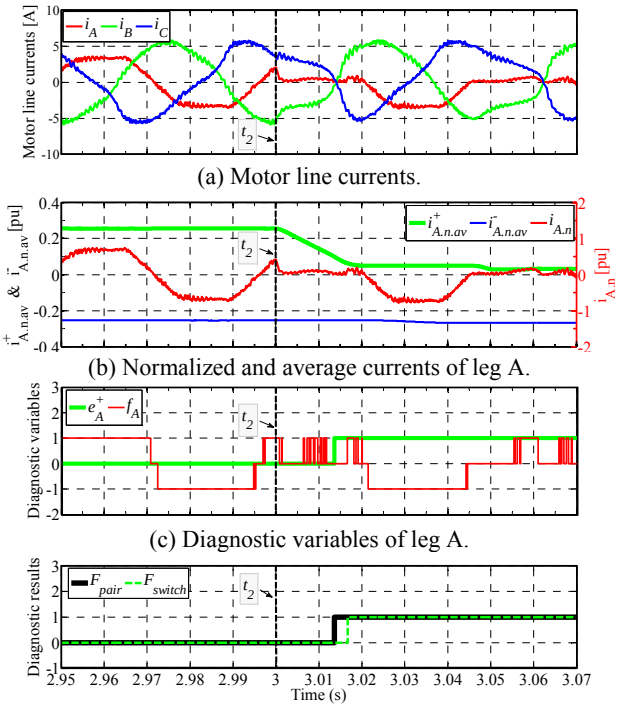

(a) Motor line currents.

(b) Normalized and average currents of leg A.

(c) Diagnostic variables of leg A.

(d) Final diagnostic results.

Fig. 12. Results for the inverter operation with an OC fault in S_{A1} and with an unbalanced load.

Zooms of Fig. 11(b) and Fig. 11(c) around t=3 s are presented in Fig. 12(a) and Fig. 12(b), respectively. As can be observed in Fig. 12(a), before the occurrence of the IGBT fault (t<3 s), the motor line currents are unbalanced (due to the motor fault), while $i^+_{A.n.av}[k] \approx 0.255$ pu and $i^-_{A.n.av}[k] \approx -0.255$ pu (Fig. 12(b)). After the appearance of the fault, the value of $i^+_{A.n.av}[k]$ decreases and becomes smaller than the threshold I^{th1+}_{av}. Therefore, $e^+_A[k]$ changes to 1 (at t=3.0136 s), as shown in Fig. 12(c). Based on this value, and considering TABLE IV, F_{pair} is identified as pair 1 and S_{A1} is identified as the faulty switch as soon as $f_A[k]$ changes to 1 for the first time (at t=3.0167 s).

The final diagnostic results are shown in Fig. 12(d). These results, which were obtained under an enormous unbalance in the motor line currents, shows that the proposed method does not give any false alarms under these conditions.

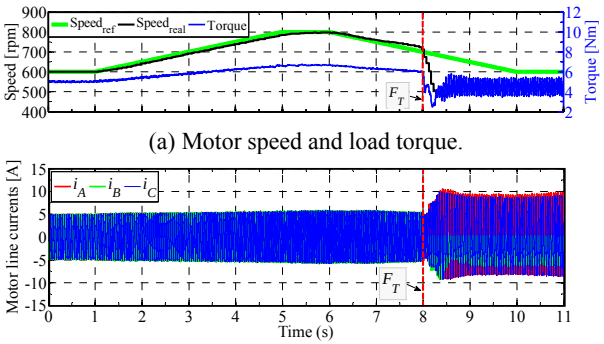

(a) Motor speed and load torque.

(b) Motor line currents.

Fig. 13. Results for two OC faults in S_{B4} and S_{B2} under transient operation.

2) Results for multiple OC faults

Several tests were also conducted for different combinations of double OC faults. Results for three different double IGBT OC faults under transient operating condition are presented. The employed reference speed profile for all of the results represented in this subsection is similar to the one shown in Fig. 6.

In the first case, results for two OC faults occurring in two IGBTs located in the same inverter leg (S_{B4} and S_{B2}) are presented. The first OC is introduced in S_{B4} at t=8 s and the second one is applied to S_{B2} at t=8.015 s.

The motor speeds and load torque evolution are shown in Fig. 13(a). The motor line current waveforms are shown in Fig. 13(b). A zoomed version of these current signals, centered at t=8 s, is presented in Fig. 14(a). The two vertical lines labeled F_T^{1st} and F_T^{2nd} indicate the instants in time when the faults in S_{B4} and S_{B2}, are introduced. Since both OC faults are located in inverter leg B, $i_{B.n}[k]$, $i^{+}_{B.n.av}[k]$ and $i^{-}_{B.n.av}[k]$ are the variables needed for the diagnostic process, and are presented in Fig. 14(b). As observed in this figure, after the occurrence of the first fault in S_{B4} at t=8 s, some of the negative values of $i_{B.n}[k]$ are eliminated and, therefore, $i^{-}_{B.n.av}[k]$ rises. Once $i^{-}_{B.n.av}[k]$ is larger than I_{av}^{th1-}, $e_B^{-}[k]$ assumes the value of 1, and the first fault is detected by the diagnostic system at t=8.011 s. According to TABLE IV, these results allow for the identification of F_{pair}=4 (P_{B2}). At this point, the behavior of $f_B[k]$ shown in Fig. 14(c), permits the identification of S_{B4} as the first faulty IGBT at t=8.0125 s.

The second OC fault is applied in S_{B2} at t=8.015 s. As can be observed in Fig. 14(b), after this moment, $i^{+}_{B.n.av}[k]$ decreases to zero. When $i^{+}_{B.n.av}[k]$ is lower than I_{av}^{th1+}, $e_B^{+}[k]$ takes the value of 1 at t=8.028 s as shown in Fig. 14(d). This allows for the identification of P_{B1} as the faulty pair.

To identify the second OC fault, it is necessary to analyze the values of $e_B^{+}[k]$ and $f_B[k]$, presented in Fig. 14(c). When $e_B^{+}[k]$ takes the value of 2 (at t=8.0335 s), the identification of S_{B2} as the second faulty IGBT is achieved.

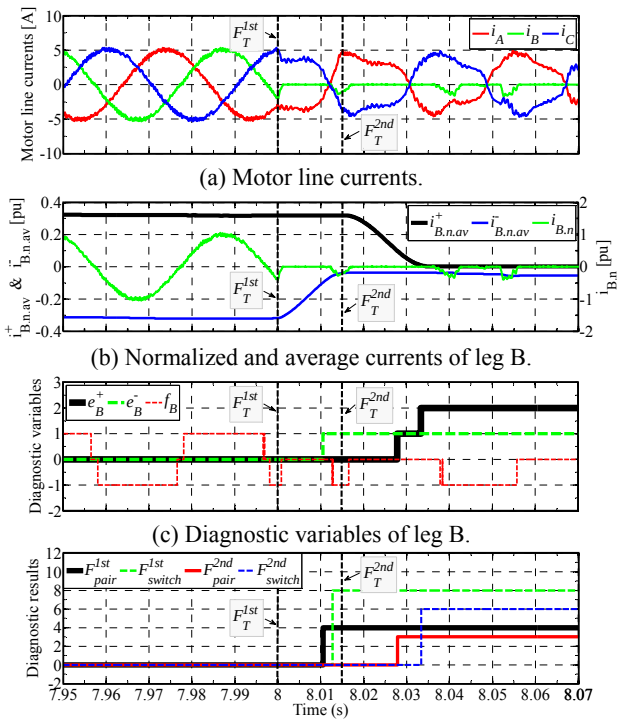

(a) Motor line currents.

(b) Normalized and average currents of leg B.

(c) Diagnostic variables of leg B.

(d) Final diagnostic results.

Fig. 14. Results for the inverter operation with two OC faults in S_{B4} and S_{B2}.

At this point, a different combination of double OC faults is analyzed for two different inverter legs. The first OC fault is applied to IGBT S_{A4} at t=8 s, and the second one is applied to IGBT S_{C1} at t=8.01 s. The motor line current waveforms are shown in Fig. 15(a).

For the OC fault in leg A, $i_{A.n}[k]$, $i^{+}_{A.n.av}[k]$ and $i^{-}_{A.n.av}[k]$ are represented in Fig. 15(b). Following the procedures previously mentioned, at t=8.0115 s $e_A^{-}[k]$=1, which allows for the identification of the faulty pair P_{A2}. Fig. 15(c) also shows that after fault detection, $f_A[k]$ takes the value of -1 at t=8.012 s. With these collected values for F_{pair} and $f_A[k]$, the identification of S_{A4} is accomplished.

For the OC fault in leg C, $i_{C.n}[k]$, $i^{+}_{C.n.av}[k]$ and $i^{-}_{C.n.av}[k]$ are represented in Fig. 15(d). Fig. 15(e), shows that at t=8.017 s $e_C^{+}[k]$ takes the value of 1, and TABLE IV allows for the identification of F_{pair}=P_{C1}. Since at the moment of the fault detection $f_C[k]$=1, S_{C1} is identified as the second faulty IGBT.

For the third case, another combination of double OC faults is analyzed. The first OC fault is applied to IGBT S_{A4} at t=8 s (similar to the previous example) and the second one is applied to IGBT S_{C2} at t=8.01 s. The motor line current waveforms are represented in Fig. 16(a).

The procedure to identify the first faulty IGBT is similar to that in the previous example.

To analysis the second OC fault, $i_{C.n}[k]$, $i^{+}_{C.n.av}[k]$ and $i^{-}_{C.n.av}[k]$ are represented in Fig. 16(d). This figure shows that

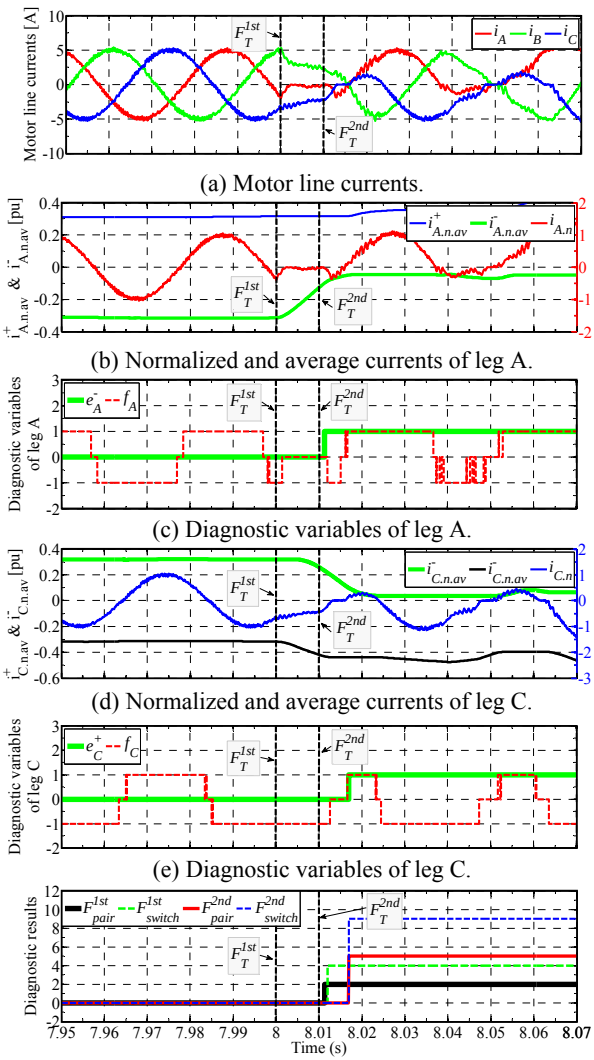

(a) Motor line currents.

(b) Normalized and average currents of leg A.

(c) Diagnostic variables of leg A.

(d) Normalized and average currents of leg C.

(e) Diagnostic variables of leg C.

(f) Final diagnostic results.

Fig. 15. Results for the inverter operation with two OC faults in S_{A4} and S_{C1}.

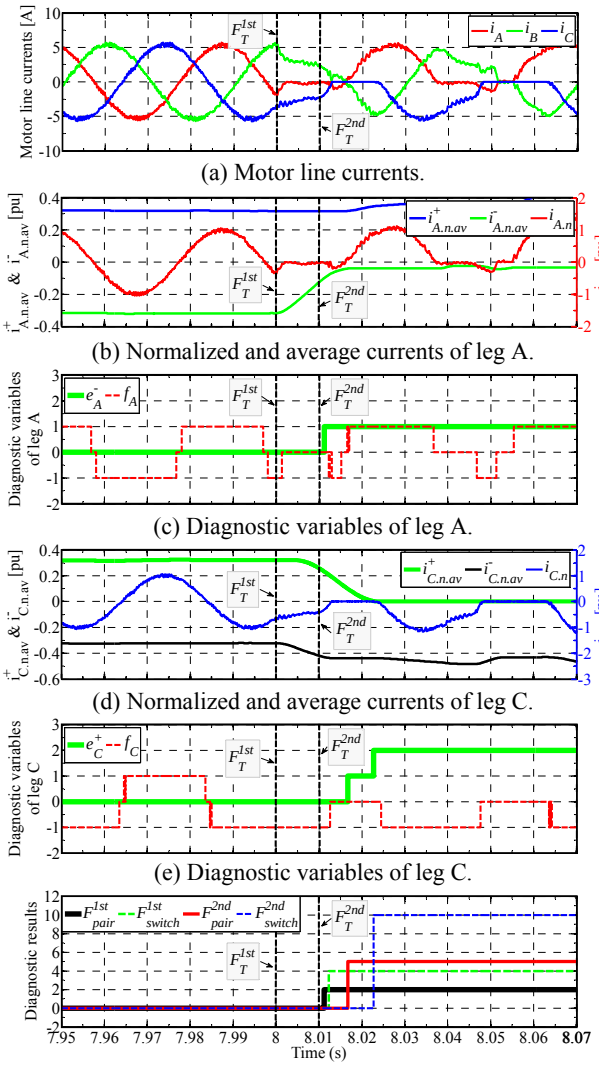

(a) Motor line currents.

(b) Normalized and average currents of leg A.

(c) Diagnostic variables of leg A.

(d) Normalized and average currents of leg C.

(e) Diagnostic variables of leg C.

(f) Final diagnostic results.

Fig. 16. Results for the inverter operation with two OC faults in S_{A4} and S_{C2}.

after the fault in S_{C2}, $i^+_{C.n.av}[k]$ decreases to below I^{th1+}_{av} at t=8.017 s. Therefore, $e^+_C[k]$ takes the value of 1, and TABLE IV allows for the identification of P_{C1} as the second faulty pair.

To identify the IGBT with the OC fault, $e^+_C[k]$ and $f_C[k]$ are shown in Fig. 16(e), at the moment $e^+_C[k]$ takes the value of 2 (t=8.023 s), and independently of $f_C[k]$ value, TABLE V give the results of S_{C2} as the second faulty IGBT. Fig. 16(f) represents the summary of the diagnostic results for this double OC fault.

If a double OC fault occurs in the IGBTs of any other inverter leg, the procedure to identify the faulty IGBT is similar to the one previously explained. TABLE VI summarizes the time taken by the diagnostic algorithm to detect and identify the faulty IGBTs in the experimental tests.

As can be seen, for all of the inverter fault operations, the diagnostic is performed within half a period of the fundamental motor line currents.

TABLE VI
DIAGNOSTIC TIMES OF THE PROPOSED APPROACH

Faulty IGBT(s)	Identification time after OC fault(s) occurrence			
	First F_{pair}	First F_{switch}	Second F_{pair}	Second F_{switch}
A_1	11.5 ms	16.6 ms	---	---
A_2	11.5 ms	17.5 ms	---	---
A_1 (unbalanced load)	13.6 ms	16.7 ms	---	---
B_4, B_2	11 ms	12.5 ms	13 ms	18.5 ms
A_4, C_1	11.5 ms	12 ms	7 ms	7 ms
A_4, C_2	11.5 ms	12 ms	7 ms	13 ms

3) *Results for load variation*

The proposed diagnostic method was also tested for a load variation. The motor runs at 500 rpm with no load. At t=0.48 s, the load changes to 5 Nm. The results are shown in Fig. 17, where the load changing instant is marked with a vertical line labeled T_v. The torque and speed variations are shown in Fig.

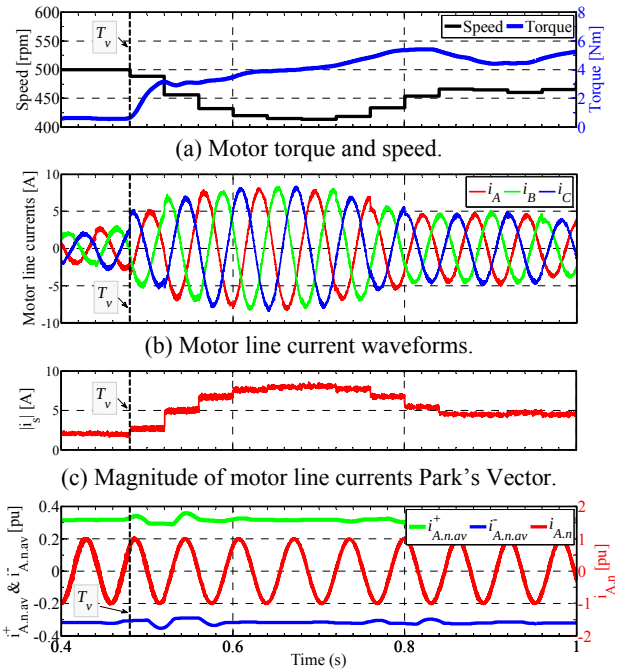

Fig. 17. Results for the inverter operation under a torque variation between no load and 5 Nm, without fault.

17(a). As can be seen in Fig. 17(b), there is a large increase in the motor line currents. It can also be seen that there are large oscillations.

As already explained (see equation (2)), the motor line current waveforms are normalized by dividing to the magnitude of the motor line currents Park's Vector, presented in Fig. 17(c). As an example, $i_{A.n}[k]$, $i^+_{A.n.av}[k]$ and $i^-_{A.n.av}[k]$ are represented in Fig. 17(d), which shows that their values are slightly affected by the load variation. However, despite this transient condition, $i^+_{A.n.av}[k]$ and $i^-_{A.n.av}[k]$ are far from the corresponding threshold values of $I^{th1+}_{av} = 0.1$ and $I^{th1-}_{av} = -0.1$. Therefore, there is a sufficient safety margin to avoid any false alarms due to load variation conditions.

V. CONCLUSIONS

This paper proposes a new approach for fault diagnosis in 3LNPC induction motor drives based on the average values of the positive and negative parts of the normalized motor line currents. This method is able to diagnose multiple OC faults in all of the controlled power switches of the inverter.

Its implementation only requires two motor line currents, which are already used by the AC drive controller. Therefore, it does not require the installation of any additional hardware or sensors. Thus, guaranteeing a low implementation cost and ease of integration into motor drive control systems.

Typically, the faulty IGBT is isolated within half of a fundamental inverter output period. The experimental results obtained with the proposed diagnostic approach under transient conditions show that this approach works well under all conditions without any incorrect results. Furthermore, the capability of the method is verified under unbalanced load operating conditions.

The proposed method has several advantages such as its ability to detect and identify multiple OC faults in all of the controlled power switches without the need for extra sensors. This diagnostic method also possess independence from the working conditions, easy implementation and reliable performance under transient working conditions.

ACKNOWLEDGMENT

The authors wish to acknowledge the financial support of the Portuguese Foundation for Science and Technology (FCT) under project number SFRH/BD/101111/2014.

REFERENCES

[1] C. L. Xia, Z. Xu, and J. X. Zhao, "A new direct power control strategy for NPC three-level voltage source rectifiers using a novel vector influence table method," *Journal of Power Electronics*, Vol. 15, No. 1, pp. 106-115, Jan. 2015.

[2] S. Kouro, M. Malinowski, K. Gopakumar, J. Pou, L. G. Franquelo, W. Bin, J. Rodriguez, M. A. Perez, and J. I. Leon, "Recent advances and industrial applications of multilevel converters," *IEEE Trans. Ind. Electron.*, Vol. 57, No. 8, pp. 2553-2580, Aug. 2010.

[3] P. Alemi, S. Y. Jeong, and D. C. Lee, "Active damping of LLCL filters using PR control for grid-connected three-level T-type converters," *Journal of Power Electronics*, Vol. 15, No. 3, pp. 786-795, May 2015.

[4] H. Abu-Rub, J. Holtz, J. Rodriguez, and G. Baoming, "Medium-voltage multilevel converters; state of the art, challenges, and requirements in industrial applications," *IEEE Trans. Ind. Electron.*, Vol. 57, No. 8, pp. 2581-2596, Aug. 2010.

[5] D. M. Lee, J. W. Jung, and S. S. Kwak, "Simple space vector PWM scheme for 3-level NPC inverters including the overmodulation region," *Journal of Power Electronics*, Vol. 11, No. 5, pp. 688-696, Sep. 2011.

[6] Z. Ye, Y. Xu, F. Li, X. Deng, and Y. Zhang, "Simplified PWM strategy for neutral-point-clamped (NPC) three-level converter," *Journal of Power Electronics*, Vol. 14, No. 3, pp. 519-530, May 2014.

[7] S. Alepuz, A. Calle, S. Busquets-Monge, S. Kouro, and B. Wu, "Use of stored energy in PMSG rotor inertia for low-voltage ride-through in back-to-back NPC converter-based wind power systems," *IEEE Trans. Ind. Electron.*, Vol. 60, No. 5, pp. 1787-1796, May 2013.

[8] G. Xiaoqiang, M. C. Cavalcanti, A. M. Farias, and J. M. Guerrero, "Single-carrier modulation for neutral-point-clamped inverters in three-phase transformerless photovoltaic systems," *IEEE Trans. Power Electron.*,Vol. 28, No. 6, pp. 2635-2637, Jun. 2013.

[9] I. Lopez, S. Ceballos, J. Pou, J. Zaragoza, J. Andreu, I. Kortabarria, and V. Agelidis, "Modulation strategy for multiphase neutral-point-clamped converters," *IEEE Trans.*

Power Electron., Vol. 31, No. 2, pp. 928-941, Feb. 2016.
[10] U. M. Choi, H. G. Jeong, K. B. Lee, and F. Blaabjerg, "Method for detecting an open-switch fault in a grid-connected NPC inverter system," *IEEE Trans. Power Electron.*, Vol. 27, No. 6, pp. 2726-2739, Jun. 2012.
[11] W. S. Im, J. S. Kim, J. M. Kim, D. C. Lee, and K. B. Lee, "Diagnosis methods for IGBT open switch fault applied to 3-Phase AC/DC PWM converter," *Journal of Power Electronics*, Vol. 12, No. 1, pp. 120-127, Jan. 2012.
[12] L. M. A. Caseiro and A. M. S. Mendes, "Real-time IGBT open-circuit fault diagnosis in three-level neutral-point-clamped voltage-source rectifiers based on instant voltage error," *IEEE Trans. Ind. Electron.*, Vol. 62, No. 3, pp. 1669-1678, Mar. 2015.
[13] U. M. Choi, F. Blaabjerg, and K. B. Lee, "Study and handling methods of power IGBT module failures in power electronic converter systems," *IEEE Trans. Power Electron.*, Vol. 30, No. 5, pp. 2517-2533, May 2015.
[14] W. Zhang, D. Xu, P. N. Enjeti, H. Li, J. T. Hawke, and H. S. Krishnamoorthy, "Survey on fault-tolerant techniques for power electronic converters," *IEEE Trans. Power Electron.*, Vol. 29, No. 12, pp. 6319-6331, Dec. 2014.
[15] Y. J. Ko and K. B. Lee, "Fault diagnosis of a voltage-fed PWM inverter for a three-parallel power conversion system in a wind turbine," *Journal of Power Electronics*, Vol. 10, No. 6, pp. 686-693, Nov. 2010.
[16] T. J. Kim, W. C. Lee, and D. S. Hyun, "Detection method for ppen-circuit fault in neutral-point-clamped inverter systems," *IEEE Trans. Ind. Electron*., Vol. 56, No. 7, pp. 2754-2763, Jul. 2009.
[17] J. S. Lee, K. B. Lee, and F. Blaabjerg, "Open-switch fault detection method of a back-to-back converter using NPC topology for wind turbine systems," *IEEE Trans. Ind. Appl.*,Vol. 51, No. 1, pp. 325-335, Jan./Feb. 2015.
[18] M. B. Abadi, A. M. S. Mendes, and S. M. A. Cruz, "Three-level NPC inverter fault diagnosis by the average current Park's vector approach," in *20th International Conference on Electrical Machines(ICEM)*, pp. 1893-1898, Sep. 2012.
[19] A. M. S. Mendes, M. B. Abadi, and S. M. A. Cruz, "Fault diagnostic algorithm for three-level neutral point clamped AC motor drives, based on the average current Park's vector," *IET Power Electronics*, Vol. 7, No. 5, pp. 1127-1137, May 2014.
[20] B. Wu, *High-Power Converters and AC Drives*, New Jersey: John Wiley & Sons. 2006.
[21] A. K. Jain and V. T. Ranganathan, "Vce sensing for IGBT protection in NPC three level converters; causes for spurious trippings and their elimination," *IEEE Trans. Power Electron*., Vol. 26, No. 1, pp. 298-307, Jan. 2011.
[22] B. R. O. Baptista, M. B. Abadi, A. M. S. Mendes, and S. M. A. Cruz, "The performance of a three-phase induction motor fed by a three-level NPC converter with fault tolerant control strategies," in 9th IEEE International Symposium on Diagnostics for Electric Machines, Power Electronics and Drives (SDEMPED), pp. 497-504, Aug. 2013.

Mohsen Bandar Abadi was born in Iran. He received his Diploma in Electrical Engineering from the University of Mashhad, Mashhad, Iran; and his M.S. degree in Electrical Engineering from the University of Semnan, Semnan, Iran. He is presently working towards his Ph.D. in the Faculty of Electrical Engineering, University of Coimbra, Coimbra, Portugal. His current research interests include wind energy conversion systems, multilevel converters, and electrical machines, with special emphasis on fault diagnosis.

André M. S. Mendes (IEEE S'95, M'05) was born in Portugal. He received his Diploma, his M.S. degree, and his Ph.D. degree in Electrical Engineering from the University of Coimbra, Coimbra, Portugal, in 1993, 1998, and 2005, respectively. Since 1991, he has been with the Department of Electrical and Computer Engineering, University of Coimbra, where he is currently an Assistant Professor and the Director of the Power Electronics Laboratory. He is also the Coordinator of the Power Systems Research Group of the Instituto de Telecomunicações, Coimbra, Portugal. His teaching interests include electrical machines and power electronics, his research interests are focused on electric power quality, fault diagnosis and the fault tolerance of electric drives and power electronic converters. Dr. Mendes is a member of the Portuguese Engineers Association (ODE).

Sérgio M. A. Cruz received his Diploma, his M.S. degree, and his Ph.D. degree in Electrical Engineering from the University of Coimbra, Coimbra, Portugal, in 1994, 1999, and 2004, respectively. He is with the Department of Electrical and Computer Engineering, University of Coimbra, where he is currently an Assistant Professor and the Director of the Electric Machines Laboratory. He is the author of more than 80 journal and conference papers. His current research interests include power transformers, rotating electric machines, electric drives, and power electronic converters, with special emphasis on fault diagnosis, fault tolerance, and digital control.